JACS
JOURNAL OF THE AMERICAN CHEMICAL SOCIETY

ARTICLE

pubs.acs.org/JACS

Biocompatible Functionalization of Polymersome Surfaces: A New Approach to Surface Immobilization and Cell Targeting Using Polymersomes

Stefan Egli,[†] Martin G. Nussbaumer,[†] Vimalkumar Balasubramanian,[†] Mohamed Chami,[‡] Nico Bruns,[†] Cornelia Palivan,[†] and Wolfgang Meier*[,†]

[†]Department of Chemistry, University of Basel, Klingelbergstrasse 80, 4056 Basel, Switzerland

[‡]Centre for Cellular Imaging and Nano Analytics, Biozentrum, University of Basel, Mattenstrasse 26, 4058 Basel, Switzerland

Supporting Information

ABSTRACT: Vesicles assembled from amphiphilic block copolymers represent promising nanomaterials for applications that include drug delivery and surface functionalization. One essential requirement to guide such polymersomes to a desired site in vivo is conjugation of active, targeting ligands to the surface of preformed self-assemblies. Such conjugation chemistry must fulfill criteria of efficiency and selectivity, stability of the resulting bond, and biocompatibility. We have here developed a new system that achieves these criteria by simple conjugation of 4-formylbenzoate (4FB) functionalized polymersomes with 6-hydrazinonicotinate acetone hydrazone (HyNic) functionalized antibodies in aqueous buffer. The number of available amino groups on the surface of polymersomes composed of poly(dimethylsiloxane)-*block*-poly(2-methyloxazoline) diblock copolymers was investigated by reacting hydrophilic succinimidyl-activated fluorescent dye with polymersomes and evaluating the resulting emission intensity. To prove attachment of biomolecules to polymersomes, HyNic functionalized enhanced yellow fluorescent protein (eYFP) was attached to 4FB functionalized polymersomes, resulting in an average number of 5 eYFP molecules per polymersome. Two different polymersome−antibody conjugates were produced using either antibiotin IgG or trastuzumab. They showed specific targeting toward biotin-patterned surfaces and breast cancer cells. Overall, the polymersome−ligand platform appears promising for therapeutic and diagnostic use.

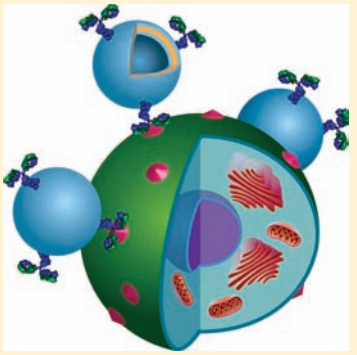

INTRODUCTION

Because of their considerable potential, nanoscale vesicles composed of block copolymers, that is, nanovesicles or polymersomes, continue to draw wide interest in diverse areas of nanotechnology and medical research.[1,2] In drug delivery, for example, cargo-carrying polymersomes that target and attach to specific cells will lead to greater drug efficacy and to fewer side effects. In the field of biosensing, for example, in ELISA assays, polymersome−antibody conjugates have, due to their high loading capacity, the potential to provide a marked advantage to nanosensor design by providing elevated sensitivities as they report specific attachment to a variety of antigens, or to complementary species in general.

To achieve their promised potential in areas such as those indicated above, it is essential that nanovesicles be subject to both precise control of design and functionality, and that they exhibit stability. In drug delivery, nanosize vesicles have been shown to possess far greater load-carrying capacity as compared to simple drug−polymer conjugates for medicinal therapy.[3] This capacity can be used for direct, site-specific transport of hydrophilic drug cargos such as doxorubicin[4] and pravastatin,[5] but also of proteins and nucleic acids.[6−8] Block copolymer vesicles are leading candidates for such nanosize applications because they feature superior membrane stability, select impermeability, precise chemical control, and a resulting structural versatility that yields a prodigious variety of possible sizes and functionalities.[9]

To be effective in drug delivery, nanovesicles must maximize three essential features: (1) membrane impermeability to a hydrophilic cargo to prevent loss of drug;[3] (2) reduced adhesion of protein to the outer surface to avoid elimination by the immune system and thus to increase circulation time in blood;[10] and (3) stable attachment of ligands that specifically target receptors of diseased cells.[11] Polymersomes based on poly(dimethylsiloxane)−poly(2-methyloxazoline) block copolymers possess these three properties[10,12] and have therefore been used in ligand-interaction, cell uptake, and nanoreactor studies.[11,13,14]

To avoid possible interactions between targeting ligands and cargo (drugs, RNA, etc.) and to prevent interference with self-assembly, attachment of ligands must take place on the outer polymersome surface after vesicle formation. Several approaches to attach ligands have been reported, for example,

Received: November 16, 2010
Published: March 03, 2011

dx.doi.org/10.1021/ja110275f | J. Am. Chem. Soc. 2011, 133, 4476–4483

biotin−streptavidin binding[11,13,15−17] or azide−alkyne click chemistry.[18,19] Although these approaches have proven feasible, they exhibit problems in terms of application in therapy, including human intolerance to streptavidin and toxic effects due to possible copper residues used to catalyze the alkyne−azide click reaction. Therefore, the challenge was to devise a biocompatible conjugation chemistry that would lead not only to precise control and stable chemical bonding but also to high selectivity while avoiding disadvantageous reaction additives and catalysts.

Various studies have clearly shown that different species such as proteins and nucleic acids can be conjugated to each other by a hydrazinonicotinamide- and a formylbenzamide-counterpart functionality, resulting in a bis-aryl hydrazone bond.[20−24] This bond is known to be biocompatible,[25] stable and selective,[20] and thus fulfilled our requirements. The reaction is efficient under mild conditions in aqueous buffer at room temperature.[20] Moreover, an inherent advantage that follows is the ability to trace and quantify the formation of the covalent link between conjugated species due to the absorbance of the formed bis-aryl hydrazone bond.

To achieve our goal, we synthesized poly(dimethylsiloxane)-*block*-poly(2-methyloxazoline) (PDMS-*b*-PMOXA) diblock copolymers with hydroxyl or piperazyl functionalities at the hydrophilic terminus. The piperazyl group represents a secondary amine, which can react with amine-targeting linkers. These diblock copolymers were used to form polymersomes with surface-exposed amine groups. The number of exposed amines on the surface was controlled by varying the molar percentage of piperazyl functional polymer, as shown by attachment of a succinimidyl ester-activated fluorophore.

We therefore applied this linker chemistry for the first time to form covalent attachment of biological ligands, such as proteins and antibodies, to the surface of polymersomes by means of the bis-aryl hydrazone bond. Using two different polymersome−antibody conjugates, we also demonstrate the specific targeting of biotin-functionalized surfaces as well as in vitro targeting of human epidermal growth factor receptor 2 (HER2),[26] which is expressed by SKBR3 human breast cancer cells.

RESULTS AND DISCUSSION

Block Copolymer Synthesis and Characterization. We synthesized PDMS-*b*-PMOXA diblock copolymers to provide a polymer with amphiphilic properties suitable for the formation of polymersomes. As compared to the PMOXA-*b*-PDMS-*b*-PMOXA triblock copolymers previously studied by our group,[8] these diblock copolymers have a more defined composition due to their narrower distribution of molecular weights. Additionally, the unreacted PDMS can be easily separated from the diblock copolymer by centrifugation, which makes purification of the diblock copolymers more efficient.

The polymerization of the hydrophilic PMOXA block from an activated PDMS was carried out as previously reported.[12,27] In our previous work, the cationic ring-opening polymerization of 2-methyl-2-oxazoline from the preactivated PDMS was ultimately quenched using a KOH solution in methanol, resulting in a hydroxyl-terminated PMOXA block. We obtained a secondary amine-terminated diblock copolymer (AB−NH) using piperazine instead of KOH as the nucleophile to quench the reaction.[28] Additionally, a hydroxyl terminated diblock copolymer (AB−OH) was synthesized. The structures of both are shown in Scheme 1.

Scheme 1. PDMS-*b*-PMOXA Diblock Copolymer Structures, One Having Hydroxyl (1, AB−OH) and the Other Piperazyl Functionality (2, AB−NH) at the Hydrophilic End

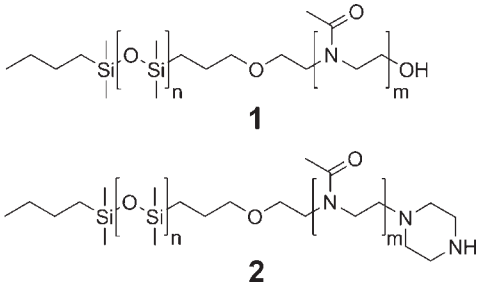

Unreacted piperazine and other low molecular weight impurities were removed by ultrafiltration in ethanol. We calculated the average composition of the block copolymers from ^{1}H NMR integral data (Supporting Information, Table S2 and Figures S1−S3). Accordingly, the hydroxyl-terminated polymer was shown to be composed of 65 siloxane units and 13 2-methyloxazoline units, and the piperazinyl-terminated polymer is composed of 68 siloxane units and 11 2-methyloxazoline units. The yield of piperazine functional groups was calculated as 82%. These values correspond to a molar mass of 6139 g mol^{-1} for AB−OH and 6185 g mol^{-1} for AB−NH. The polydispersity index M_w/M_n of the polymers was measured by GPC, where calculations were based on polystyrene standards. M_w/M_n of PDMS was found to be 1.10, that of AB−OH was 1.51, and for AB−NH it was 1.66. These values are slightly lower than those of triblock copolymers published previously.[27,29,30]

Polymersome Formation and Characterization. Polymersomes were formed using the film hydration method.[31] We determined the dimensions of the extruded polymersomes by dynamic and static light scattering (DLS, SLS).[32] Corresponding data are shown in Table 1 and as a Guinier plot in Supporting Information, Figure S5. From these values, we obtain the ρ-value given as $\rho = R_g/R_h$, which provides information on the internal structure of our particles in solution.[33]

Because the ρ-value for an ideal hollow sphere (i.e., vesicle) is 1.0 and for solid spheres is 0.775,[33] the ρ-values of our samples, at 0.92 for AB−OH and 0.95 for AB−NH, indicate hollow-sphere morphologies. From the molecular weights of the polymer itself and of its aggregated structures, we calculated the aggregation numbers (N_{agg}) for AB−NH and AB−OH. They agreed well with those of PMOXA-*b*-PMDS-*b*-PMOXA triblock copolymers published previously.[27,34] Transmission electron microscopy (TEM) and cryo-TEM investigations were performed to confirm vesicular structures. Collapsed polymersomes can be seen in the TEM micrograph, and in cryo-TEM images we recognize the polymersome membrane (Figure 1).

The diameters of polymersomes observed in a cryo-TEM image are, in most cases, smaller than those found in TEM images. The reason for this can be attributed to the preparation of the negative stain TEM sample, which causes drying and thus flattening of the polymersomes, whereas cryo-TEM conserves the native structure because the polymersomes are imaged in the frozen-hydrated state. Inclusions present in some polymersomes are smaller vesicles and micelles. The average membrane thickness of 50 different polymersomes in cryo-TEM images was measured as 15.4 ± 0.7 nm, which is more than 3 times thicker than phospholipid bilayers from liposomes. Thus, we conclude

Table 1. Light Scattering Data of AB−OH and AB−NH in Aqueous Solution

polymer	R_h, nm	PDI[a]	R_g, nm	M_w, g mol^{-1}	A_2, mol dm^3 g^{-2}	N_{agg}	ρ-value
AB−OH	96.5	0.12	89.2 ± 0.6	1.66×10^8	5.51×10^{-10}	2.70×10^4	0.92
AB−NH	96.4	0.09	91.6 ± 0.4	6.92×10^7	3.65×10^{-10}	1.12×10^4	0.95

[a] The polydispersity index from light scattering data represents the error of R_h.

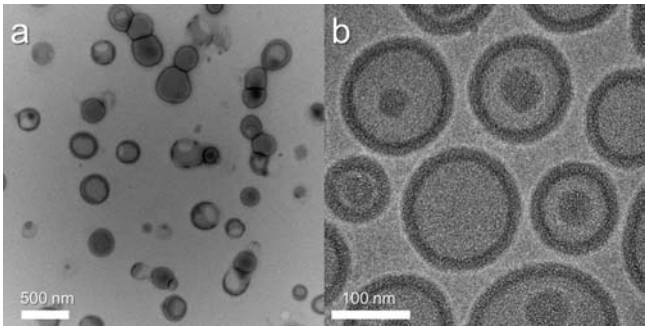

Figure 1. TEM (a) and cryo-TEM (b) micrographs of AB−OH polymersomes in water.

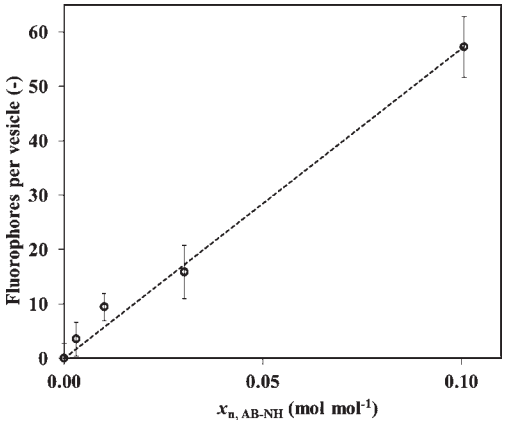

Figure 2. Average number of covalently conjugated fluorophore molecules per polymersome versus the molar percentage of AB−NH. The data were corrected for unspecific adsorption of fluorophores.

that the relatively thick polymer membrane as well as the inclusions inside the polymersomes (Figure 1b) might explain the small deviation of ρ-values calculated from light scattering data from the ideal ρ-value for vesicles.

Effects on Polymersome Surface Functionalization. Understanding and controlling the binding site density of reactive ligands on polymersome surfaces is of great importance for applications such as targeted drug delivery.[35,36] To investigate the effects of functional group concentration on polymersome surface modification, we produced different batches of polymersomes consisting of varying molar percentages of the reactive AB−NH and the AB−OH diblock copolymers. Next, a simple fluorescent dye was conjugated to the amine end groups. We decided to use the bright, photostable dye, Alexa Fluor 633 carboxylic acid, activated as succinimidyl ester (A633−NHS), as the ligand for these binding site studies, due to its excellent fluorescence quantum yield and good solubility in aqueous solution. Becausee it was previously shown that such NHS reactive fluorophores bind to secondary amines,[37,38] we assume that the majority of available AB−NH binding sites are modified after incubation in a large excess of NHS reactive Alexa dye. Because the NHS group of the fluorophore hydrolyzes quickly in aqueous buffer at higher pH values,[39] an excess of activated dye was required to ensure that accessible amines on the polymersome surface reacted with the ligand within an appropriate time. After complete reaction of polymersomes with A633−NHS, the samples were extensively dialyzed and finally investigated using fluorescence correlation spectroscopy (FCS). In contrast to conventional fluorescence spectroscopy, FCS enables the accurate detection of the diffusion time and brightness of single vesicles.[13] Diffusion times τ_D = 44 ± 4 μs for freely diffusing A633−NHS and τ_D = 5.7−9.6 ms for polymersome−A633 conjugates were measured. This indicates successful binding of A633−NHS to the polymersomes. The brightness of the polymersomes, and thus the degree of ligand functionalization on the polymersome surface, was derived from the fluorescence intensity trace. Six samples of each AB−NH mol % were measured to obtain statistical and representative values. By dividing the average polymersome brightness value by the average brightness of a single dye molecule, we obtained the average number of fluorophores per polymersome. In a sample consisting of 100 mol % of AB−OH and 0 mol % of AB−NH polymer, we measured a fluorescence intensity corresponding to 7.6 ± 0.9 fluorophores per polymersome. We assigned this value to represent unspecific binding of the polyaromatic fluorophore to the polymersome membrane and thus subtracted it from all other values given below. In Figure 2, the interdependence of the average number of fluorophores per polymersome (N_{FP}) and the mole percentage of AB−NH ($x_{n,\ AB-NH}$) are illustrated.

Values from 0.3 to 10 mol % AB−NH fit a linear function well, which is shown by $N_{FP} = 569.2x_{n,\ AB-NH}$ (R^2 = 0.991), quantitatively describing the number of fluorophores per polymersome. Errors in fluorescence intensity (Figure 2) originate basically with polymersome size distribution. A saturation of dye attachment to the polymersome was observed at higher molar percentages of AB−NH, from 10 to 100 mol %. This saturation can be explained by steric hindrance by dye molecules that were already attached to the polymersome surface. Additionally, we assume that at higher $x_{n,AB-NH}$ phase separation of dye-modified and nonmodified block copolymers in the membrane occurs,[40] which enhances steric hindrance to further dye conjugation and causes fluorescence quenching.[41] This assumption is supported by the observation of some large aggregates (with diameters up to 10 μm) found in laser scanning micrographs (Supporting Information, Figure S8) and indicates a destabilization and thus aggregation of the original self-assemblies. Because the illuminated sampling volume is rather small, the size-limiting criterion for FCS measurements being less than 1 μm^3,[42] as compared to those aggregates, it was not possible to obtain representative FCS results for samples containing more than 10 mol % AB−NH.

The yield of the conjugation reaction can be estimated from the equation above, and the N_{agg} value can be obtained from light scattering data. N_{agg} was measured to be 11 200 diblock copolmer molecules per polymersome. Thus, about 5600 of them are

in the outer part of the polymersome bilayer membrane. In the linear range up to 10 mol % of AB−NH, the conjugation efficiency is 10%. At first view, this conjugation efficiency might be considered poor. However, by taking into account that a large excess of reagent was used and that some of the functional groups are presumably concealed in the hydrophilic corona of the polymersome, this conjugation efficiency in fact represents the surface-accessible NH-groups.

A further argument in favor of covalent binding of A633−NHS to AB−NH polymer is given by FCS diffusion measurements of polymersomes dried by lyophilization and redissolved in ethanol, in which polymersomes disassemble into individual diblock copolymers. Thus, we determined the τ_D of free A633−NHS and of the AB−NH−A633 conjugates. For A633−NHS ($M \approx 1200$ g mol^{-1}, 5.3 nM), we measured a τ_D of 91.8 ± 1.0 μs, and for the AB−NH−A633 conjugate (0.1 μg mL^{-1}), a τ_D of 155.8 ± 2.2 μs was found, which results in a theoretical molecular weight for the AB−NH−A633 conjugate of 5866 ± 248 g mol^{-1}. This molecular weight agrees well with M_n of AB−NH diblock copolymer obtained from ^{1}H NMR measurements and indicates successful covalent bonding. FCS diffusion measurements of a mixture of A633−NHS (5.3 nM) and AB−OH (0.1 μg mL^{-1}) in ethanol were performed to ensure that the fluorophore was attached exclusively by covalent bonds and not by nonspecific interactions with AB−NH. The resulting τ_D of 104.6 ± 1.4 μs corresponds to a theoretical molecular weight of 1775 ± 71 g mol^{-1}, which allowed us to assume that only a few, nonspecific, noncovalent bindings occurred. These experiments point out that our polymersomes were covalently functionalized with NHS reactive fluorophores in aqueous solution in a controlled, reproducible manner. However, because we assumed that phase separation occurs at a higher molar percentage of modified AB−NH (≥10 mol %), we ultimately used polymersomes that contained 3 mol % AB−NH in further conjugation reactions.

Covalent Attachment of Enhanced Yellow Fluorescent Protein to Polymersomes. Simple and efficient attachment of ligands to preformed membranes is of great importance. For drug delivery purposes, not only is the attachment of relatively small sugars and peptides as targeting moieties of interest, but so is the conjugation of large proteins and antibodies to the polymersome surface. We decided to use a conjugation strategy that resulted in a stable and quantifiable bis-aryl hydrazone bond based on two complementary heterobifunctional linkers[20] (Scheme 2).

As compared to other conjugation techniques, this method works under mild conditions in aqueous buffers at pH values between 4.5 and 8.0; more importantly, it does not require the use of toxic catalysts such as, for example, Cu(I), which is required for azide−alkyne click chemistry in aqueous solution.[18,19,43] In previous studies, this conjugation chemistry was used to covalently attach biomolecules such as antibodies and oligonucleotides to each other.[20,44] However, to our knowledge, it has not been used previously to modify polymeric self-assemblies and, in particular, not for the modification of block copolymer membranes.

Because of its fluorescent properties, eYFP was used as a model protein ligand in our experiment. As outlined in Scheme 2, polymersomes were modified with succinimidyl 4-formylbenzoate (NHS−4FB), and the ligand was modified with succinimidyl 6-hydrazinonicotinate acetone hydrazone (NHS−HyNic). We did not modify the polymers with 4FB before the self-assembly to polymersomes, to avoid possible interactions between the fluorescent dye and the 4FB group. Also, we kept the percentage of

Scheme 2. Conjugation Reaction Scheme of 4-Formylbenzoate-Modified Polymersomes with 6-Hydrazinonicotinate Acetone Hydrazone-Modified Ligands (e.g., Protein or Antibody) Resulting in a Covalent and Stable Bis-aryl Hydrazone Bond

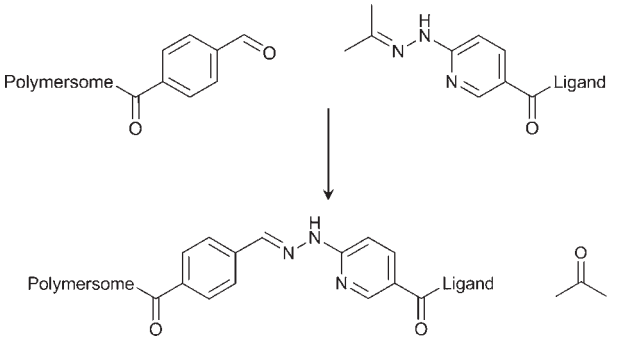

reactive AB−NH polymer low, at 3 mol %, to avoid the attachment of more than one polymersome to eYFP. The 4FB functionalization of polymersomes was confirmed by a colorimetric reaction with 2-hydrazinopyridine and by gel permeation chromatography of the polymer, as shown in the Supporting Information, Figure S4b and S9. Functional succinimidyl 4-hydrazinonicotinate acetone hydrazone (S−HyNic) groups, being complementary reactive parts to the 4FB-modified polymersomes, were introduced to the eYFP.[20] The two conjugation partners, the polymersomes and eYFPs, were incubated in phosphate buffer, pH 6.0, for 16 h. The absorption of the resulting bis-aryl hydrazone bond between the polymersome and eYFP was below the detection limit, due to increased scattering of the polymersomes at lower wavelength, and could therefore not be detected via ultraviolet−visible (UV−vis) spectroscopy.

Because eYFP, with it is almost a perfect cylindrical shape of 42 Å by 24 Å,[45] is smaller by an order of magnitude than polymersomes having an average diameter of 193 nm, we used FCS as a suitable method to investigate the binding of proteins to polymersomes.[13] The average τ_D for free eYFP in solution was found to be 93 ± 3 μs, and for eYFP−polymersome conjugates it was 3.98 ± 0.57 ms. This difference in τ_D is clearly shown in the shift of the FCS autocorrelation curves (Figure 3).

The FCS autocorrelation curve of the eYFP−polymersome conjugate was analyzed by a nonlinear least-squares fitting program,[13] assuming one population of fluorescent species. This indicates binding of eYFP to the polymersome. Using the τ_D for eYFP and for polymersome−eYFP conjugates along with the known diffusion coefficient D of fluorescent GFPs and YFPs,[46] the theoretical R_h of the polymersome−-eYFP conjugate was calculated using the relationship between τ_D and D from FCS[13] and the Stokes−Einstein equation. Assuming, in a first approximation, the eYFP and the polymersomes to be spherical, we calculated an R_h of 2.3 ± 0.1 nm for eYFP, and 98.3 ± 14.1 nm for the eYFP−polymersome conjugate. A diameter of eYFP−polymersome conjugates of approximately 200 nm is further evidence for covalent attachment of eYFP to the polymersomes. Polymersomes without benzaldehyde functional groups on their surfaces did not conjugate to eYFP (τ_D of 93 ± 3 μs). We calculated the average brightness of freely diffusing eYFP and compared it to the brightness of eYFP−polymersome conjugates. An average number of 5 eYFP per polymersome was

determined, which is significantly lower than the number of, for example, noncovalently bound streptavidin to biotin-modified polymeric vesicles.[13] As shown above, A633−NHS-modified polymersomes consisting of the same molar percentage of AB−NH had, on average, 17 covalently attached dye molecules per polymersome. The number of eYFP ligands was found lower by a factor of 3. This could be due to the difference in sizes of the protein and fluorescent dye.

Polymersome−Antibody Conjugates for Specific Surface Targeting. Because of their specific, strong binding to proteins and haptens, antibodies are ideal candidates as targeting ligands.[47] We functionalized antibodies with HyNic moieties and attached them covalently to 4FB modified polymersomes, similar to the method as described for polymersome−eYFP conjugates. In the first trial, HyNic-modified antibiotin IgG was attached to 4FB-modified polymersomes consisting of 3 wt % AB−NH and containing the fluorescent dye Alexa Fluor 647 maleimide (A647-M) encapsulated inside the polymersome cavity. The polymersome−antibody conjugates were incubated on a glass slide, which was previously patterned with biotinylated bovine serum albumin (BSA) by a microcontact printing process.[48] To avoid unspecific binding, the glass surface of the pattern interspaces was passivated with nonbiotinylated BSA. The surface was imaged by confocal laser scanning microscopy. As shown in Figure 4, the polymersome−antibody conjugates bonded specifically to the biotinylated pattern printed on the glass slide. As control experiments, polymersome−anti-RBC−IgG conjugates were synthesized and applied to patterned surfaces (Figure 4c). No specific binding of the polymersomes to biotinylated surface area was observed.

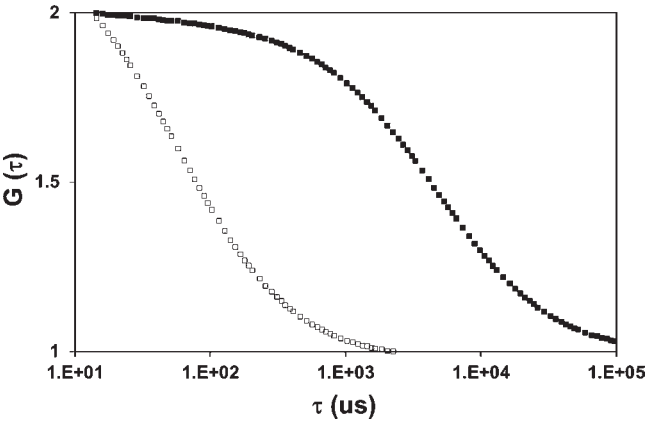

Figure 3. Fitted FCS autocorrelation curve of free eYFP (□) and polymersome−eYFP conjugate (■).

The packing density of immobilized polymersomes in Figure 4a and b on the glass substrate was sufficiently low to be able to recognize dots that possibly represent single immobilized polymersomes. This is due to the fact that every antibody exhibits only three HyNic functionalities on average, which could also be positioned at the active antibody binding site.[49] Therefore, some antibodies might be covalently attached, with their active binding site facing the polymersome surface, and thus might not be able to bind to the biotin-BSA pattern presented on the glass surface. Their specific antigen targeting properties and their high fluorescence intensities render polymersome−antibody conjugates ideal candidates for biosensor applications such as enzyme-linked immunosorbent assays (ELISA). When employing conventional antibody−dye conjugates, an optimum in labeling should be found between underconjugation, resulting in a fluorescence signal that is too low, and overconjugation, resulting in a change in antigen-binding characteristics and potentially inactivating the antibody completely with fluorophores.[50] In comparison to those conventional labeled antibodies, the sensitivity of ELISA should be increased several-fold by introducing polymersome−antibody conjugates, due to their high loading capacity with fluorescent molecules.

Targeted Uptake of Polymersome−Trastuzumab Conjugates. Targeted polymersomes have been shown to be ideal candidates to transport drugs specifically to diseased cells.[11] Because conjugates of trastuzumab with cytotoxic agents have been proven to specifically target HER2-positive breast cancer cells and considerably improve the therapeutic index,[51] we decided to use polymersome−trastuzumab conjugates for cell targeting. SKBR3 cells incubated for 2 h with sulforhodamine-B-containing polymersome−trastuzumab conjugates and sulforhodamine-B-containing polymersomes without trastuzumab, as the negative control, were analyzed for qualitative uptake with CLSM (Figure 5). To distinguish the extracellular and intracellular region of the cells, the cell membrane was stained with Deep Red. We observed polymersome−trastuzumab conjugates located intracellularly, and few were present in the cell membrane (Figure 5).

Very low uptake of polymersomes without trastuzumab as compared to polymersome−trastuzumab conjugates was observed under similar conditions. This clearly indicates a fast and specific targeted uptake of polymersome−trastuzumab conjugates in SKBR3 cells. The targeting effect mediated by trastuzumab to HER2 receptors expressed on SKBR3 cell is significant at short incubation times, for example, 2 h. For a long incubation time (24 h), the difference between polymersomes with and without trastuzumab was not distinguishable, due to the nonspecific uptake of polymersomes without trastuzumab.

The quantitative uptake of sulforhodamine B containing polymersome−trastuzumab conjugates in SKBR3 cells was

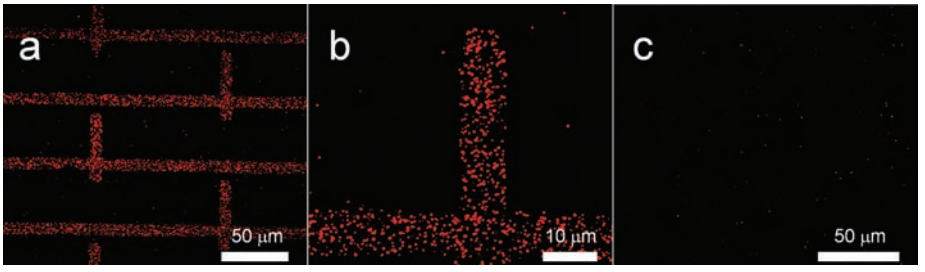

Figure 4. CLSM micrographs of (a) A647-M containing polymersomes with covalently attached antibiotin IgG, immobilized on a biotin-BSA pattern; (b) close-up view of (a); and (c) A647-M containing polymersomes with covalently attached antierythrocyte IgG conjugates.

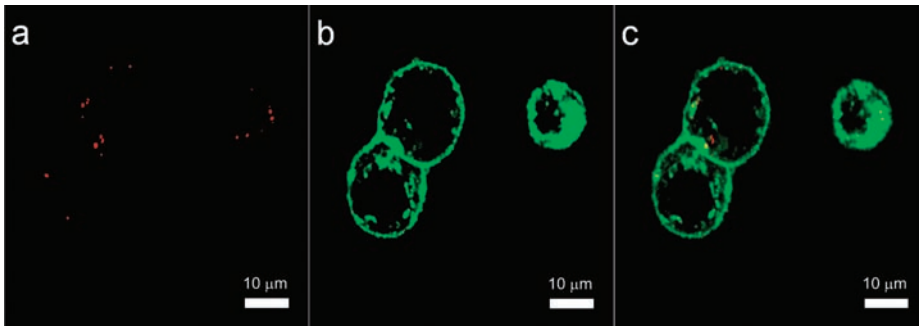

Figure 5. CLSM micrograph of SKBR3 cells after 2 h incubation with polymersome−trastuzumab conjugate, which encapsulated sulforhodamine B. (a) Polymersome−trastuzumab located intracellularly and in the cell membrane, shown in the red channel; (b) SKBR3 cell membrane stained with Deep Red, shown in the green channel; and (c) overlay of the micrographs from the red and green channels.

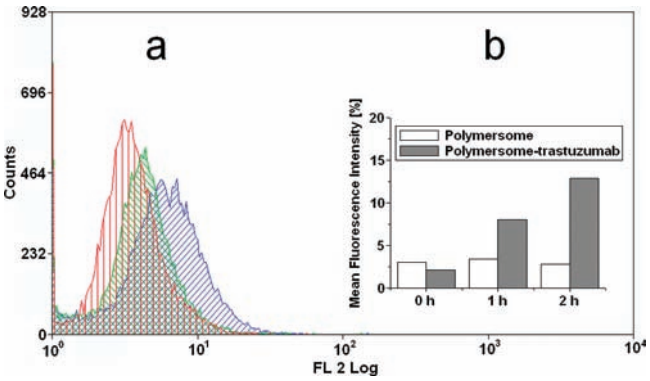

Figure 6. Flow cytometry analysis. (a) Histogram of SKBR3 cells (red), SKBR3 cells incubated 2 h with sulforhodamine-B-containing polymersomes (green), and SKBR3 cells incubated 2 h with sulforhodamine-B-containing polymersome−trastuzumab conjugate (blue); and (b) mean fluorescent intensity of SKBR3 cells, incubated with sulforhodamine-B-containing polymersomes with and without conjugated trastuzumab for 1 and 2 h.

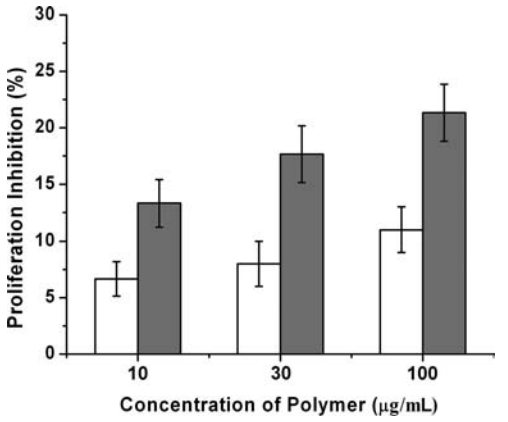

Figure 7. MTS assay. Proliferation inhibition effect on SKBR3 cells with different concentrations of polymersome with (gray) and without trastuzumab (white) after 24 h incubation.

analyzed with flow cytometry. The intensity of the fluorescence channel measured for cells after 1 h incubation with polymersome−trastuzumab conjugates was 8%, and it increased up to 13% after 2 h incubation, while for polymersomes without trastuzumab this was less than 3% even after 2 h. This supports the specific uptake of the polymersome−trastuzumab conjugates as being due to the presence of trastuzumab as the targeting ligand. By subtracting the auto fluorescence of cells, an uptake of polymersome−trastuzumab conjugates of approximately 10% was calculated for 2 h incubation (Figure 6).

As expected, uptake of polymersome−trastuzumab conjugates is significantly faster than that of polymersomes without trastuzumab, in agreement with other reported studies.[52] Besides, the uniform shift of the histogram in the fluorescent channel clearly indicates that the uptake is evenly distributed in the cells.

In Vitro Cell Proliferation Inhibition Activity of Polymersome−Trastuzumab Conjugates. Trastuzumab is known to inhibit proliferation of SKBR3 cells due to its specific binding to the HER2 receptor on the surface of the cells.[53] Therefore, the effect of polymersome−trastuzumab conjugates on cell proliferation was studied spectroscopically via the formation of a colored formazan product when MTS was biologically reduced by metabolically active cells.[54] After 24 h incubation, while polymersomes without trastuzumab induced an inhibition of 7−11%, polymersome−trastuzumab conjugates inhibited the proliferation in the range of 14−21% (Figure 7).

Under similar conditions, polymersome−trastuzumab conjugates were able to inhibit proliferation of SKBR3 by a factor of almost 2. In addition, polymersome−trastuzumab conjugates inhibited cell proliferation in a dose-dependent manner (Figure 7). These findings allow us to consider that the conjugation to the polymersome did not affect the functionality of the antibody. The inhibiting effect of polymersome−trastuzumab conjugates as compared to polymersomes can be further improved by modulation of the number of trastuzumab per polymersome, and in this respect further experiments are ongoing to optimize the system.

CONCLUSION

The goal of this work was to design and implement a simple, efficient, and universal method to covalently attach biological ligands, such as antibodies, to polymersomes to provide a platform for targeting experiments. New amphiphilic PDMS-*b*-PMOXA diblock copolymers comprising hydroxyl or amine functionalities at their hydrophilic ends were thereby synthesized and characterized. We were able to control covalent attachment of NHS-activated fluorescent dye to polymersomes in aqueous buffer by systematically varying the molar percentage of AB−NH in the polymersome. Polymersomes and ligands were modified

with complementary functionalities (4FB and HyNic) to attach macromolecular ligands, such as eYFP or antibodies, to the polymersome surface. Successful conjugation of eYFP to polymersomes was proven by fluorescence diffusion measurements. In a subsequent step, we attached HyNic-modified antibodies to polymersomes that were subsequently used to target selected antigens. With potential applications such as immunoassays (e.g., ELISA) in mind, polymersome antibiotin−IgG conjugates were shown to specifically target biotin-patterned glass surfaces with a virtual absence of nonspecific binding. In addition, polymersome−trastuzumab conjugates showed specific adherence to the HER2 receptor of SKBR3 breast cancer cells, as demonstrated by LSM imaging and FACS experiments. The effect of polymer concentration and incubation times on proliferation of cells was established via the MTS assay; polymersomes exhibited no significant toxicity. We do not expect any toxic effect due to the bis-aryl hydrazone bond, because it was shown elsewhere that PEGylated polyamidoamine dendrimers with bis-aryl hydrazone linkages induced no obvious cytotoxic response in HN12 tumor cells over a period of 48 h.[55] In contrast to, for example, copper-catalyzed alkyne−azide click chemistry, all procedures here, from polymersome formation to ligand attachment, can be carried out under mild, biocompatible conditions. This makes this system applicable to therapeutic application in vivo. However, further investigations on the influence of the packing density of bulky, macromolecular ligands on the polymersome surface are ongoing. These should enhance our understanding of the polymersome−ligand conjugate attachment and uptake in cells, and thus lead to greater control.

In a nutshell, this polymersome−ligand platform, based on bis-aryl hydrazone conjugation chemistry that allows multifaceted and stable attachment of targeting ligands (e.g., antibodies), presents new opportunities to make immunoassays more sensitive and drug administration more effective.

■ ASSOCIATED CONTENT

Supporting Information. Figures S1−S5 and S8−S9, experimental methods, general procedures, materials, and additional experimental data. This material is available free of charge via the Internet at http://pubs.acs.org.

■ AUTHOR INFORMATION

Corresponding Author
wolfgang.meier@unibas.ch

■ ACKNOWLEDGMENT

We thank the Swiss National Science Foundation, the NCCR Nanosciences, and the University of Basel for financial support. N.B. is grateful for a Marie-Curie Intra-European Fellowhip. We acknowledge N. E. Hynes and T. Stölzle from Friedrich Miescher Institute for providing SKBR3 cell lines, Ch. Bitter and N. Ott from University Hospital Pharmacy Basel for providing trastuzumab antibody, and the Zentrum für Mikroskopie Basel (ZMB) for access to TEM. Experimental assistance from S. Kasper, D. Häussinger, K. Jaskiewicz, I. Lieberwirth, and G. Persy is gratefully acknowledged. W.M. is thankful to P. Vajkoczy. We thank M. Inglin for editing this manuscript and R. Pfalzberger for some of the artwork.

■ REFERENCES

(1) Uchegbu, I. F. *Expert Opin. Drug Delivery* **2006**, *3*, 629.
(2) Balasubramanian, V.; Onaca, O.; Enea, R.; Hughes, D. W.; Palivan, C. G. *Expert Opin. Drug Delivery* **2010**, *7*, 63.
(3) Litvinchuk, S.; Lu, Z.; Rigler, P.; Hirt, T. D.; Meier, W. *Pharm. Res.* **2009**, *26*, 1711.
(4) Ahmed, F.; Pakunlu, R. I.; Brannan, A.; Bates, F.; Minko, T.; Discher, D. E. *J. Controlled Release* **2006**, *116*, 150.
(5) Broz, P.; Ben-Haim, N.; Grzelakowski, M.; Marsch, S.; Meier, W.; Hunziker, P. *J. Cardiovasc. Pharmacol.* **2008**, *51*, 246.
(6) Discher, D. E.; Photos, P.; Ahmed, F.; Parthasrathy, R.; Bates, F. S. *Biomed. Aspects Drug Targeting* **2002**, 459.
(7) Levine, D. H.; Ghoroghchian, P. P.; Freudenberg, J.; Zhang, G.; Therien, M. J.; Greene, M. I.; Hammer, D. A.; Murali, R. *Methods* **2008**, *46*, 25.
(8) Onaca, O.; Enea, R.; Hughes, D. W.; Meier, W. *Macromol. Biosci.* **2009**, *9*, 129.
(9) Discher, D. E.; Eisenberg, A. *Science* **2002**, *297*, 967.
(10) Konradi, R.; Pidhatika, B.; Muehlebach, A.; Textor, M. *Langmuir* **2008**, *24*, 613.
(11) Broz, P.; Benito, S. M.; Saw, C.; Burger, P.; Heider, H.; Pfisterer, M.; Marsch, S.; Meier, W.; Hunziker, P. *J. Controlled Release* **2005**, *102*, 475.
(12) Kumar, M.; Grzelakowski, M.; Zilles, J.; Clark, M.; Meier, W. *Proc. Natl. Acad. Sci. U.S.A.* **2007**, *104*, 20719.
(13) Rigler, P.; Meier, W. *J. Am. Chem. Soc.* **2006**, *128*, 367.
(14) Axthelm, F.; Casse, O.; Koppenol, W. H.; Nauser, T.; Meier, W.; Palivan, C. G. *J. Phys. Chem. B* **2008**, *112*, 8211.
(15) Ben-Haim, N.; Broz, P.; Marsch, S.; Meier, W.; Hunziker, P. *Nano Lett.* **2008**, *8*, 1368.
(16) Lin, J. J.; Ghoroghchian, P. P.; Zhang, Y.; Hammer, D. A. *Langmuir* **2006**, *22*, 3975.
(17) Robbins, G. P.; Saunders, R. L.; Haun, J. B.; Rawson, J.; Therien, M. J.; Hammer, D. A. *Langmuir* **2010**, *26*, 14089.
(18) Opsteen, J. A.; Brinkhuis, R. P.; Teeuwen, R. L. M.; Loewik, D. W. P. M.; van Hest, J. C. M. *Chem. Commun.* **2007**, 3136.
(19) van Dongen, S. F. M.; Nallani, M.; Cornelissen, J. J. L. M.; Nolte, R. J. M.; van Hest, J. C. M. *Chem.-Eur. J.* **2009**, *15*, 1107.
(20) Bruns, N.; Pustelny, K.; Bergeron, L. M.; Whitehead, T. A.; Clark, D. S. *Angew. Chem., Int. Ed.* **2009**, *48*, 5666.
(21) Hartmann, D. M.; Heller, M.; Esener, S. C.; Schwartz, D.; Tu, G. *J. Mater. Res.* **2002**, *17*, 473.
(22) Chen, Y.; Aveyard, J.; Wilson, R. *Chem. Commun.* **2004**, 2804.
(23) Zhong, X.-b.; Reynolds, R.; Kidd, J. R.; Kidd, K. K.; Jenison, R.; Marlar, R. A.; Ward, D. C. *Proc. Natl. Acad. Sci. U.S.A.* **2003**, *100*, 11559.
(24) Steinberg-Tatman, G.; Huynh, M.; Barker, D.; Zhao, C. *Bioconjugate Chem.* **2006**, *17*, 841.
(25) Walker, G. F.; Fella, C.; Pelisek, J.; Fahrmeir, J.; Boeckle, S.; Ogris, M.; Wagner, E. *Mol. Ther.* **2005**, *11*, 418.
(26) Baselga, J. *Eur. J. Cancer* **2001**, *37*, S18.
(27) Nardin, C.; Hirt, T.; Leukel, J.; Meier, W. *Langmuir* **2000**, *16*, 1035.
(28) Bonne, T. B.; Luedtke, K.; Jordan, R.; Stepanek, P.; Papadakis, C. M. *Colloid Polym. Sci.* **2004**, *282*, 833.
(29) Nardin, C.; Winterhalter, M.; Meier, W. *Langmuir* **2000**, *16*, 7708.
(30) Kita-Tokarczyk, K.; Itel, F.; Grzelakowski, M.; Egli, S.; Rossbach, P.; Meier, W. *Langmuir* **2009**, *25*, 9847.
(31) Battaglia, G.; Ryan, A. J. *J. Phys. Chem. B* **2006**, *110*, 10272.
(32) Jin, A. J.; Huster, D.; Gawrisch, K.; Nossal, R. *Eur. Biophys. J.* **1999**, *28*, 187.
(33) Stauch, O.; Schubert, R.; Savin, G.; Burchard, W. *Biomacromolecules* **2002**, *3*, 565.
(34) Kita-Tokarczyk, K.; Grumelard, J.; Haefele, T.; Meier, W. *Polymer* **2005**, *46*, 3540.
(35) Martin, A. L.; Li, B.; Gillies, E. R. *J. Am. Chem. Soc.* **2009**, *131*, 734.
(36) Stahn, R.; Zeisig, R. *Tumor Biol.* **2000**, *21*, 176.
(37) Cline, G. W.; Hanna, S. B. *J. Am. Chem. Soc.* **1987**, *109*, 3087.

(38) Gruber, H. J.; Kada, G.; Pragl, B.; Riener, C.; Hahn, C. D.; Harms, G. S.; Ahrer, W.; Dax, T. G.; Hohenthanner, K.; Knaus, H. G. *Bioconjugate Chem.* **2000**, *11*, 161.
(39) Nojima, Y.; Iguchi, K.; Suzuki, Y.; Sato, A. *Biol. Pharm. Bull.* **2009**, *32*, 523.
(40) Christian, D. A.; Tian, A.; Ellenbroek, W. G.; Levental, I.; Rajagopal, K.; Janmey, P. A.; Liu, A. J.; Baumgart, T.; Discher, D. E. *Nat. Mater.* **2009**, *8*, 843.
(41) Duportail, G. *Springer Ser. Fluoresc.* **2005**, *3*, 133.
(42) Starchev, K.; Zhang, J.; Buffle, J. *J. Colloid Interface Sci.* **1998**, *203*, 189.
(43) Evans, C. E.; Lovell, P. A. *Chem. Commun.* **2009**, 2305.
(44) Kozlov, I. A.; Melnyk, P. C.; Stromsborg, K. E.; Chee, M. S.; Barker, D. L.; Zhao, C. *Biopolymers* **2004**, *73*, 621.
(45) Craggs, T. D. *Chem. Soc. Rev.* **2009**, *38*, 2865.
(46) Petrasek, Z.; Schwille, P. *Biophys. J.* **2008**, *94*, 1437.
(47) Patel, R. P.; Patel, G.; Patel, N. A. *Pharma Rev.* **2008**, *6*, 144.
(48) Delamarche, E. *Chimia* **2007**, *61*, 126.
(49) Wakankar, A. A.; Feeney, M. B.; Rivera, J.; Chen, Y.; Kim, M.; Sharma, V. K.; Wang, Y. J. *Bioconjugate Chem.* **2010**, *21*, 1588.
(50) Vira, S.; Mekhedov, E.; Humphrey, G.; Blank, P. S. *Anal. Biochem.* **2010**, *402*, 146.
(51) Hughes, B. *Nat. Rev. Drug Discovery* **2010**, *9*, 665.
(52) Wuang, S. C.; Neoh, K. G.; Kang, E.-T.; Pack, D. W.; Leckband, D. E. *Biomaterials* **2008**, *29*, 2270.
(53) Longva, K. E.; Pedersen, N. M.; Haslekas, C.; Stang, E.; Madshus, I. H. *Int. J. Cancer* **2005**, *116*, 359.
(54) Malich, G.; Markovic, B.; Winder, C. *Toxicology* **1997**, *124*, 179.
(55) Yuan, Q.; Yeudall, W. A.; Yang, H. *Biomacromolecules* **2010**, *11*, 1940.